Elastic electron scattering formalism for relativistic nuclear models*

L. D. Miller†

Laboratory for Nuclear Science and Department of Physics, Massachusetts Institute of Technology, Cambridge, Massachusetts 02139

(Received 11 August 1975; revised manuscript received 22 April 1976)

The classical static equation of motion for a relativistic vector field interacting through direct and derivative coupling with a spinor source term is presented in spherical coordinates. The equation is generalized to include the effects of form factors at the vector-spinor vertices. Using appropriate nucleon electromagnetic form factors and nuclear single-particle wave functions resulting from relativistic self-consistent model calculations of spherical nuclei, the contributions of the various components of the nucleon electromagnetic form factors to the effective nuclear charge distributions and the elastic electron scattering cross sections for ^{40}Ca, ^{48}Ca, and ^{208}Pb are analyzed.

[NUCLEAR STRUCTURE Electromagnetic form factors, relativistic formalism, ρ and $\sigma(\theta)$ calculated for elastic scattering of electrons off ^{40}Ca, ^{48}Ca, and ^{208}Pb.]

I. INTRODUCTION

The existence of relativistic self-consistent nuclear models which reproduce the experimental bulk properties of finite spherical nuclei[1,2] make it possible to study in a natural and intuitive way the contributions of the various nucleon electromagnetic form factors (Dirac and Pauli) to effective nuclear charge distributions. The Dirac form factor of the proton will, of course, provide the dominant contribution; however, the remaining contributions (mainly the neutron and proton Pauli form factors) may be important in understanding fine details of the elastic electron scattering cross sections of nuclei. These relativistic contributions, which have been investigated previously within a nonrelativistic reduction, have been shown to be important in understanding the isotopic shift anomaly in the ^{40}Ca-^{48}Ca isotopes.[3]

The appropriate relativistic formalism is most easily obtained by considering the static classical equations of motion for a spinor field interacting with a vector field via both direct and derivative coupling. Since the aim is to calculate effective charge distributions for spherical nuclei, it is convenient to consider the equations of motion directly in spherical coordinates. Once these equations have been reduced to radial form, it becomes obvious how one should introduce the nucleon electromagnetic form factors by folding the appropriate point nucleon densities with their respective coordinate space nucleon form factors.

The five parameter, monopole, $\Gamma_\rho = 0$, vector dominance model of Iachello, Jackson, and Lande[4] has been used for the nucleon electromagnetic form factors. This model, which produces a respectable fit to the experimental data (χ^2 of 1.75 per data point), results in coordinate space Dirac and Pauli form factors which are linear combinations of Yukawa functions. These are very convenient for folding with the relativistic point nucleon densities to obtain effective nuclear charge distributions.

Application of the relativistic formalism to the ^{40}Ca-^{48}Ca isotopes yields somewhat different results from those obtained in Ref. 3. One difference is that the exact cancellation of the Pauli form factor (analog of the spin-orbit term of Ref. 3) for spin saturated shells does not persist in the relativistic formalism. The cancellation is still significant, however, since the Pauli form factor contributions to the spin saturated ^{40}Ca nucleus are much smaller than those contributions to the spin unsaturated ^{48}Ca nucleus. Complicating this discussion is the fact that there is also significant cancellation between the proton and neutron Pauli form factors.

In Ref. 3 the relativistic corrections were not sufficient to remove the entire discrepancy between the theoretical and experimental isotopic shifts of ^{40}Ca-^{48}Ca. In the present work the relativistic contributions are larger, and the discrepancy between theory and experiment takes a different sign from that of Ref. 3. This difference is more likely due to differences in the nuclear models used in Ref. 3 and the present work rather than to differences in the formalisms.

For ^{208}Pb the results with the present model are interesting in that they give an effective charge distribution with a definite central depression, which was suggested some time ago[5] on the basis of the experimental cross section. In the present model the central depression results because the Pauli form factor contributions near the origin are particularly strong and remove the s-state bump which is present in the Dirac form factor

contribution of the protons. The Dirac form factor contribution of the neutrons in ^{208}Pb is negligible.

II. THEORY

The derivation of the static equations of motion for a vector field interacting through direct and derivative coupling with a static radially symmetric fermion distribution requires careful attention to the conventions of relativity and tensor analysis. It is appropriate to begin this section with a careful exposition of the particular conventions employed in this work.

The metric employed for the rectangular coordinate system $(x^0 = ct, x^1, x^2, x^3)$ is

$$(g_{\mu\nu}) = \begin{bmatrix} 1 & 0 & 0 & 0 \\ 0 & -1 & 0 & 0 \\ 0 & 0 & -1 & 0 \\ 0 & 0 & 0 & -1 \end{bmatrix}. \tag{1}$$

The usual tensor transformation rules for contravariant and covariant tensors are employed,

$$\bar{a}^{rs} = \frac{\partial \bar{x}^r}{\partial x^t}\,\frac{\partial \bar{x}^s}{\partial x^u}\,a^{tu}, \quad \bar{a}_{st} = \frac{\partial x^u}{\partial \bar{x}^s}\,\frac{\partial x^u}{\partial \bar{x}^t}\,a_{uv}. \tag{2}$$

The summation convention is employed over all symbols which occur once as contravariant and once as covariant indices. The relativistic spherical coordinates $(\bar{x}^0 = x^0,\ \bar{x}^1 = r, \bar{x}^2 = \theta,\ \bar{x}^3 = \phi)$ are introduced, where

$$\begin{aligned} x^0 &= \bar{x}^0 \\ x^1 &= r\sin\theta\cos\phi, \\ x^2 &= r\sin\theta\sin\phi, \\ x^3 &= r\cos\theta\,. \end{aligned} \tag{3}$$

The contravariant and covariant components of the metric tensor in the spherical coordinates become

$$(\bar{g}^{\mu\nu}) = \begin{bmatrix} 1 & 0 & 0 & 0 \\ 0 & -1 & 0 & 0 \\ 0 & 0 & -1/r^2 & 0 \\ 0 & 0 & 0 & -1/r^2\sin^2\theta \end{bmatrix},$$

$$(\bar{g}_{\mu\nu}) = \begin{bmatrix} 1 & 0 & 0 & 0 \\ 0 & -1 & 0 & 0 \\ 0 & 0 & -r^2 & 0 \\ 0 & 0 & 0 & -r^2\sin^2\theta \end{bmatrix}. \tag{4}$$

Since this metric tensor is not constant, one finds the following nonzero Christoffel symbols:

$$\begin{Bmatrix} 2 \\ 12 \end{Bmatrix} = \begin{Bmatrix} 2 \\ 21 \end{Bmatrix} = \begin{Bmatrix} 3 \\ 13 \end{Bmatrix} = \begin{Bmatrix} 3 \\ 31 \end{Bmatrix} = \frac{1}{r}\,,$$

$$\begin{Bmatrix} 3 \\ 23 \end{Bmatrix} = \begin{Bmatrix} 3 \\ 32 \end{Bmatrix} = \cot\theta\,,$$

$$\begin{Bmatrix} 1 \\ 22 \end{Bmatrix} = -r\,, \tag{5}$$

$$\begin{Bmatrix} 1 \\ 33 \end{Bmatrix} = -r\sin^2\theta\,,$$

$$\begin{Bmatrix} 2 \\ 33 \end{Bmatrix} = -\sin\theta\cos\theta\,,$$

where

$$\begin{Bmatrix} r \\ mn \end{Bmatrix} = g^{rp}[mn,p]\,, \tag{6}$$

and

$$[mn,p] = \frac{1}{2}\left(\frac{\partial g_{np}}{\partial x^m} + \frac{\partial g_{pm}}{\partial x^n} - \frac{\partial g_{mn}}{\partial x^p}\right). \tag{7}$$

Covariant differentiation of a tensor is denoted by a comma preceeding the index of the coordinate with respect to which differentiation is performed:

$$A_{r,s} = \frac{\partial A_r}{\partial x^s} - \begin{Bmatrix} m \\ rs \end{Bmatrix} A_m\,. \tag{8}$$

The contravariant components of the Dirac γ matrix in rectangular coordinates are

$$(\gamma^\mu) = (\gamma^0, \vec{\gamma}),\ \gamma^0 = \begin{pmatrix} I & 0 \\ 0 & -I \end{pmatrix}, \qquad \vec{\gamma} = \begin{pmatrix} 0 & \vec{\sigma} \\ -\vec{\sigma} & 0 \end{pmatrix}, \tag{9}$$

where I and $\vec{\sigma}$ are the two-by-two identity and Pauli spin matrices, respectively. In spherical coordinates the γ matrices take the form

$$\begin{aligned} \bar{\gamma}^0 &= \gamma^0\,, \\ \bar{\gamma}^1 &= \gamma^r = \begin{pmatrix} 0 & \sigma_r \\ -\sigma_r & 0 \end{pmatrix}, \\ \bar{\gamma}^2 &= \gamma^\theta = \frac{1}{r}\begin{pmatrix} 0 & \sigma_\theta \\ -\sigma_\theta & 0 \end{pmatrix}, \\ \bar{\gamma}^3 &= \gamma^\phi = \frac{1}{r\sin\theta}\begin{pmatrix} 0 & \sigma_\phi \\ -\sigma_\phi & 0 \end{pmatrix}, \end{aligned} \tag{10}$$

where σ_r, σ_θ, and σ_ϕ are the spherical coordinate components of the Pauli spin matrices:

$$\sigma_r = \begin{pmatrix} \cos\theta & \sin\theta\, e^{-i\phi} \\ \sin\theta\, e^{i\phi} & -\cos\theta \end{pmatrix},$$

$$\sigma_\theta = \begin{pmatrix} -\sin\theta & \cos\theta\, e^{-i\phi} \\ \cos\theta\, e^{i\phi} & \sin\theta \end{pmatrix}, \qquad (11)$$

$$\sigma_\phi = \begin{pmatrix} 0 & -ie^{-i\phi} \\ ie^{i\phi} & 0 \end{pmatrix}.$$

Now consider the Lagrangian density of an electron field ψ_e interacting via the electromagnetic field A_μ with a static nuclear source denoted by sums over single-nucleon wave functions ψ_N through both direct and derivative coupling,

$$\mathcal{L}(x) = -\bar{\psi}_e(x)[-i\gamma^\mu \partial_\mu + m_e]\psi_e(x) - e\bar{\psi}_e(x)\gamma^\mu\psi_e(x)A_\mu(x)$$
$$- \sum_i e_{N_i}\bar{\psi}_{N_i}(x)\gamma^\mu\psi_{N_i}(x)A_\mu(x)$$
$$- \sum_i \frac{\kappa_{N_i}}{4M_N}\bar{\psi}_{N_i}(x)\sigma^{\mu\nu}\psi_{N_i}(x)[\partial_\mu A_\nu(x) - \partial_\nu A_\mu(x)]$$
$$+ \tfrac{1}{2}\partial_\mu A^\nu(x)\partial^\mu A_\nu(x), \qquad (12)$$

where

$$\sigma^{\mu\nu} = \frac{\gamma^\mu\gamma^\nu - \gamma^\nu\gamma^\mu}{2i}. \qquad (13)$$

One ordinarily derives the equations of motion for field operators from Lagrangian densities like Eq. (12) by application of the Euler-Lagrange equations

$$\frac{\partial\mathcal{L}(x)}{\partial\xi(x)} - \partial_\mu\left[\frac{\partial\mathcal{L}(x)}{\partial\partial_\mu\xi(x)}\right] = 0, \qquad (14)$$

where ξ is either the electron field operator or the electromagnetic field operator. The matrix element of the equation of motion for the electron field between the vacuum state and the one electron state yields the Dirac equation for an electron moving in the static Coulomb potential $A_0(x)$ of the nuclear source, provided one ignores the quantum fluctuation terms in the electromagnetic field. For static rotationally invariant nuclear sources, only the zeroth component of the electromagnetic field can acquire a nonzero expectation value and still satisfy all the appropriate invariance principles.

The interest of the present work is to study the equation of motion for the Coulomb potential $A_0(x)$ and isolate the effective nuclear charge distribution which generates it. Since the nuclear source is assumed to be spherically symmetrical, it is convenient to consider the equation of motion in the spherical coordinate system. Eqs. (12) and (14) must be modified in spherical coordinates to the extent that all partial derivatives of tensor quantities must be replaced by covariant derivatives, if the proper Lorentz covariance of the equations is to be maintained. The Euler-Lagrange equation for $\bar{A}_0(x)$ becomes

$$\frac{\partial\mathcal{L}(x)}{\partial\bar{A}_0(x)} - \left[\frac{\partial\mathcal{L}(x)}{\partial\bar{A}_{0,\mu}(x)}\right]_{,\mu} = 0, \qquad (15)$$

and the Lagrangian density becomes

$$\mathcal{L}(x) = -\bar{\psi}_e(x)[-i\bar{\gamma}^\mu\bar{\partial}_\mu + m_e]\psi_e(x) - e\bar{\psi}_e(x)\bar{\gamma}^\mu\psi_e(x)\bar{A}_\mu(x)$$
$$- \sum_i e_{N_i}\bar{\psi}_{N_i}(x)\bar{\gamma}^\mu\psi_{N_i}(x)\bar{A}_\mu(x)$$
$$- \sum_i \frac{\kappa_{N_i}}{4M_N}\bar{\psi}_{N_i}(x)\bar{\sigma}^{\mu\nu}\psi_{N_i}(x)[\bar{A}^{(x)}_{\nu,\mu} - \bar{A}^{(x)}_{\mu,\nu}]$$
$$+ \tfrac{1}{2}g^{\nu\beta}g^{\mu\gamma}\bar{A}_{\beta,\mu}(x)\bar{A}_{\nu,\gamma}(x). \qquad (16)$$

Application of Eq. (15) to the Lagrangian density in Eq. (16) yields

$$-[g^{\mu\gamma}\bar{A}^{(x)}_{0,\gamma}]_{,\mu} = e\bar{\psi}_e(x)\bar{\gamma}^0\psi_e(x) + \sum_i e_{N_i}\bar{\psi}_{N_i}(x)\bar{\gamma}^0\psi_{N_i}(x)$$
$$- \sum_i \frac{\kappa_{N_i}}{2M_N}[\bar{\psi}_{N_i}(x)\bar{\sigma}^{\mu 0}\psi_{N_i}(x)]_{,\mu}. \qquad (17)$$

Since the metric tensor can be treated as a constant with respect to covariant differentiation, one recognizes the left-hand side of Eq. (17) to be the negative of the second-order invariant differential operator (D'Alembertian) operating upon the Coulomb potential $\bar{A}_0(x)$. The first term on the right-hand side of Eq. (17) is the contribution to the Coulomb potential from the electron itself and should not be included in the calculation of the scattering of the electron from the nuclear source. The equation for the Coulomb potential which should be used in calculating the electron scattering cross sections is thus

$$\nabla^2\bar{A}_0(\vec{r}) = \rho_N(\vec{r}), \qquad (18)$$

where

$$\rho_N(\vec{r}) = \sum_i e_{N_i}\bar{\psi}_{N_i}(\vec{r})\bar{\gamma}^0\psi_{N_i}(\vec{r})$$
$$- \sum_i \frac{\kappa_{N_i}}{2M_N}[\bar{\psi}_{N_i}(\vec{r})\bar{\sigma}^{\mu 0}\psi_{N_i}(\vec{r})]_{,\mu} \qquad (19)$$

The expression in Eq. (19) would be the effective charge distribution of a nucleus as measured by electron scattering experiments, if the nucleons could be considered point sources of the electromagnetic field. The presence of a term proportional to the nucleon anomalous magnetic moment

in the charge distribution is associated with the fact that the wave functions ψ_N describe nucleons in motion about some fixed point even though the matter density $\psi_N^\dagger \psi_N$ is time independent. A moving magnetic dipole serves as a source for an electric field just as a moving electric dipole serves as a source for a magnetic field.

Now consider the last term of Eq. (19),

$$\sum_i \frac{\kappa_{N_i}}{2M_N}[\bar{\psi}_{N_i}(\vec{r})\bar{\sigma}^{\mu 0}\psi_{N_i}(\vec{r})]_{,\mu} = i\sum_i \frac{\kappa_{N_i}}{2M_N}[\bar{\psi}_{N_i}(\vec{r})\bar{\gamma}^0\bar{\gamma}^j\psi_{N_i}(\vec{r})]_{,j}, \tag{20}$$

where the sum over the index j runs from 1 to 3. Making use of the nonzero Christoffel symbols given in Eq. (5), one obtains the following expression for the covariant derivative on the right-hand side of Eq. (20):

$$\sum_i \frac{\kappa_{N_i}}{2M_N}[\bar{\psi}_{N_i}(\vec{r})\bar{\gamma}^0\bar{\gamma}^j\psi_{N_i}(\vec{r})]_{,j} = \sum_i \frac{\kappa_{N_i}}{2M_N}\left\{\left(\frac{\partial}{\partial r}+\frac{2}{r}\right)[\bar{\psi}_{N_i}(\vec{r})\bar{\gamma}^0\bar{\gamma}^1\psi_{N_i}(r)] + \left(\frac{\partial}{\partial\theta}+\cot\theta\right)[\bar{\psi}_{N_i}(\vec{r})\bar{\gamma}^0\bar{\gamma}^2\psi_{N_i}(\vec{r})] + \frac{\partial}{\partial\phi}[\bar{\psi}_{N_i}(\vec{r})\bar{\gamma}^0\bar{\gamma}^3\psi_{N_i}(\vec{r})]\right\}. \tag{21}$$

The proof that the last two terms of Eq. (21) vanish is reserved for Appendix A. The remaining term may be further reduced to the form

$$\sum_i \frac{\kappa_{N_i}}{2M_N}\left(\frac{\partial}{\partial r}+\frac{2}{r}\right)[\bar{\psi}_{N_i}(\vec{r})\bar{\gamma}^0\bar{\gamma}^1\psi_{N_i}(\vec{r})] = -i\sum_i \frac{\kappa_{N_i}}{M_N}\left(\frac{\partial}{\partial r}+\frac{2}{r}\right)\frac{2J_i+1}{4\pi r^2}F_i(r)G_i(r), \tag{22}$$

where $F_i(r)$ and $G_i(r)$ are the large and small component radial wave functions as defined in Refs. 1 and 2. The sum over the index i now covers the quantum numbers n, ω, J of the single particle orbitals (see Ref. 2 or Appendix A for wave function and quantum number notation), the sum over magnetic substates having been performed already. One finally obtains the following radial expression for the point nucleon effective charge distribution:

$$\rho_N(r) = \sum_i e_{N_i}\frac{2J_i+1}{4\pi r^2}\{F_i^2(r)+G_i^2(r)\} - \sum_i \frac{\kappa_{N_i}}{M_N}\left(\frac{\partial}{\partial r}+\frac{2}{r}\right)\frac{2J_i+1}{4\pi r^2}F_i(r)G_i(r). \tag{23}$$

At this point the finite size effects of the nucleons may be introduced by smearing the point nucleon densities in Eq. (23) with the appropriate electromagnetic form factors. The appropriate form factors for the relativistic formalism are the Dirac and Pauli (F_1 and F_2) form factors rather than the electric and magnetic (G_E and G_M) form factors, which are appropriate for the nonrelativistic analysis.[3] The folding of the first term of Eq. (23) with the charge (Dirac) form factors of protons and neutrons proceeds in exact analogy with the nonrelativistic treatment in which the matter distributions are folded with the electric form factor (G_E) of protons and neutrons. The folding of the second term of Eq. (23) with the Pauli (anomalous moment) form factor is not so obvious, since one appears to have the option of folding either before or after the operation of the operator $(\partial/\partial r + 2/r)$ upon the point nucleon densities. The latter option is chosen in the present work, because the former introduces an unphysical singularity in the charge density at the origin.

Application of the form factor corrections yields

$$\rho_{\text{eff}}(r) = \rho_1^p(r)+\rho_1^n(r)+\rho_2^p(r)+\rho_2^n(r), \tag{24}$$

where

$$\rho_1^p(r) = \int \sum_{\text{protons}} \frac{2J+1}{4\pi r'^2}\{F^2(r')+G^2(r')\} \times F_1^p(|\vec{r}-\vec{r}'|)d^3r', \tag{25}$$

$$\rho_1^n(r) = \int \sum_{\text{neutrons}} \frac{2J+1}{4\pi r'^2}\{F^2(r')+G^2(r')\} \times F_1^n(|\vec{r}-\vec{r}'|)d^3r', \tag{26}$$

$$\rho_2^p(r) = -\frac{1}{M_N}\int\left(\frac{\partial}{\partial r'}+\frac{2}{r'}\right) \times \sum_{\text{protons}} \frac{2J+1}{4\pi r'^2}F(r')G(r') \times F_2^p(|\vec{r}-\vec{r}'|)d^3r', \tag{27}$$

$$\rho_2^n(r) = -\frac{1}{M_N}\int\left(\frac{\partial}{\partial r'}+\frac{2}{r'}\right) \times \sum_{\text{neutrons}} \frac{2J+1}{4\pi r'^2}F(r')G(r') \times F_2^n(|\vec{r}-\vec{r}'|)d^3r'. \tag{28}$$

The $F_{1,2}^{p,n}$ functions occurring in Eqs. (25)–(28) are the Dirac and Pauli form factors pf protons and neutrons. These are the three-dimensional Four-

ier transforms of the momentum space form factors and are normalized such that the volume integrals of F_1^p and F_1^n are 1 and 0, respectively, while the volume integrals of F_2^p and F_2^n are 1.793 and -1.913 (proton and neutron anomalous magnetic moments), respectively.

III. NUCLEON FORM FACTORS AND NUCLEAR MODELS

The nucleon electromagnetic form factors of Iachello, Jackson, and Lande[4] are used for the numerical calculations presented here. Their models are based upon the vector dominance theory of electromagnetic interactions and are fitted to experimental data from all four nucleon electromagnetic form factors. They include contributions from the ρ, ω, and ϕ mesons, as well as an intrinsic contribution which simply multiplies all four factors. The particular model used here is the five parameter, $\Gamma_\rho = 0$, monopole model which gives a χ^2 of 1.75 per data point. The use of the model with zero ρ meson width is essential in maintaining simple analytic expressions for the form factors in coordinate space. The monopole model (which refers to the intrinsic part of the form factor) is chosen, since it provides the best fit of the $\Gamma_\rho = 0$ models. It also leads to a simpler expression for the form factor than does the dipole model.

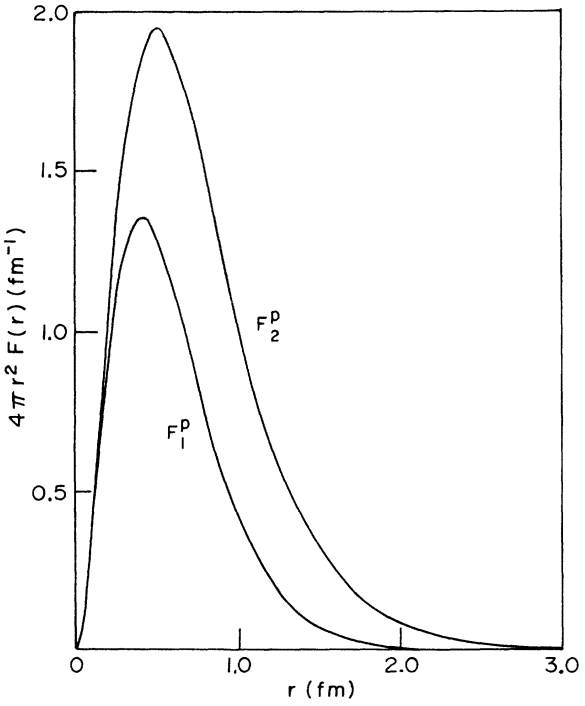

FIG. 1. The coordinate space charge (F_1^p) and anomalous magnetic moment (F_2^p) distributions of the proton.

The momentum space expressions for the form factors may be obtained from Ref. 4. Using the parameters of the chosen model and performing the Fourier transform to coordinate space, one obtains:

$$F_1^p(r) = 0.568\, e^{-3.88r}/r + 0.417\, e^{-3.98r}/r + 3.470\, e^{-5.17r}/r - 4.533\, e^{-6.30r}/r, \quad (29)$$

$$F_1^n(r) = -0.568\, e^{-3.88r}/r + 0.417\, e^{-3.98r}/r + 3.470\, e^{-5.17r}/r - 4.700\, e^{-6.30r}/r, \quad (30)$$

$$F_2^p(r) = 3.578\, e^{-3.88r}/r - 0.300\, e^{-3.98r}/r + 0.541\, e^{-5.17r}/r - 3.819\, e^{-6.30r}/r, \quad (31)$$

and

$$F_2^n(r) = -3.578\, e^{-3.88r}/r - 0.300\, e^{-3.98r}/r + 0.541\, e^{-5.17r}/r + 3.337\, e^{-6.30r}/r. \quad (32)$$

For convenience of comparison with other models, these functions (multiplied by $4\pi r^2$) are shown in Figs. 1 and 2. The simple form of these coordinate space form factors make them very convenient for folding with numerical density distributions. One may note that the Dirac form factor

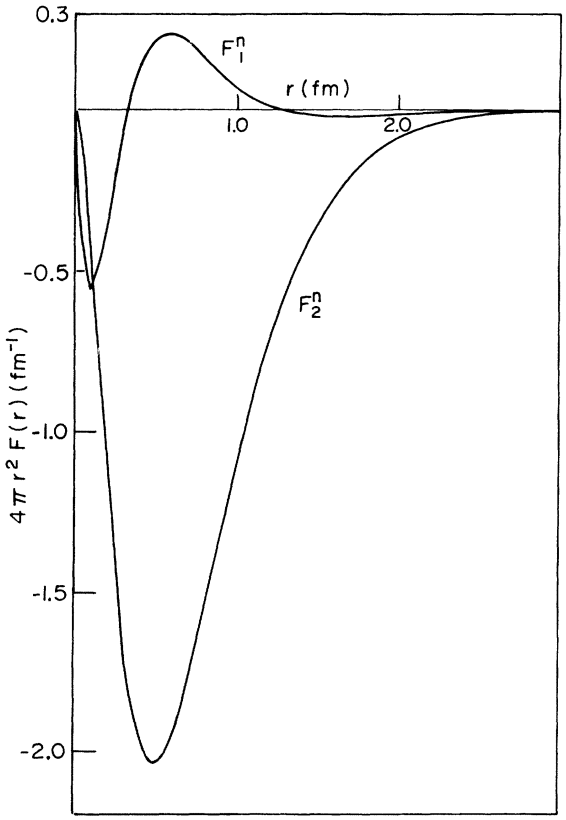

FIG. 2. The coordinate space charge (F_1^n) and anomalous magnetic moment (F_2^n) distributions of the neutron.

TABLE I. Values of the meson masses and coupling constants of the self-consistent nuclear model. The column labeled J^P refers to the spin and parity of the meson. The column labeled I refers to its isospin. The masses are given in units of MeV, and the coupling constants quoted are the conventional $g^2/4\pi$ values. For those parameters which correspond to physical mesons, the conventional symbol for the meson is included.

Meson	J^P	I	Meson mass	Coupling const.
	0^+	0	370.65	5.1604
ω	1^-	0	782.8	15.0
ρ	1^-	1	763.0	1.455
	1^-	0	135.0	0.0878

of the neutron is much smaller than the other form factors. Indeed, this is the form factor which, as noted by Foldy,[6] contributes almost nothing to the scattering of neutrons off bound atomic electrons and may even be rigorously zero.

The self-consistent nuclear model for the present calculations is a relativistic Hartree model which differs from the model used for the calculations in Ref. 1 only in that different parameters have been chosen for the effective nucleon-nucleon interaction. The model parameters which are characterized as effective masses and coupling constants of exchanged bosons are listed in Table I. It should be noted that only two of the four mesons in Table I correspond to physically observed mesons. The parameters of Table I are chosen such that the binding energy per particle of balanced nuclear matter is 16 MeV at the minimum of the saturation curve which occurs at $k_f = 1.24$ fm^{-1}. The symmetry coefficient is 31.5 MeV. These numbers are calculated with the relativistic Hartree formalism for infinite nuclear matter which was developed by Walecka.[7] Since the main purpose of the present work is to display and illustrate the relativistic form factor formalism rather than to discuss the dynamics of the relativistic self-consistent model, further consideration of the relativistic Hartree formalism is reserved for Appendix B.

IV. CALCULATIONS

The bulk properties of the doubly magic nuclei ^{40}Ca, ^{48}Ca, and ^{208}Pb, resulting from relativistic Hartree calculations with the model parameters shown in Table I, are given in Table II. The experimental total binding energies are taken from the standard mass tables.[8] The experimental rms charge radii are taken from the paper of Frosch *et al.*[9] for the Ca isotopes and from Heisenberg *et al.*[5] for ^{208}Pb.

By inspection of the rms radii of the Ca isotopes in Table II, one can begin to compare the results of the present work with Ref. 3, where similar effects were calculated with a nonrelativistic formalism. In Ref. 3 the contribution of the spin-orbit term to the effective nuclear charge density vanishes except when spin unsaturated shells are occupied. Such an exact cancellation does not obtain in the relativistic formalism; nevertheless, one sees that in ^{40}Ca the rms charge radius remains unchanged to four significant figures when the Pauli form factor contributions and the Dirac form factor contribution of neutrons are added. In Ref. 3 the rms charge radius of ^{48}Ca decreases by 0.021 fm when the spin-orbit and charge form factor contributions of the $f\frac{7}{2}$ neutrons are included. For the present work one notes that the ^{48}Ca rms radius decreases by 0.052 fm when the Pauli form factor contributions and the neutron Dirac form factor contribution are added to the proton Dirac form factor contribution. This is roughly twice the effect found in Ref. 3. For the nuclear model used in Ref. 3,[10] the point proton radius of ^{48}Ca is 0.04 fm larger than the point proton radius of ^{40}Ca. The reduction of 0.021 fm in the ^{48}Ca charge radius found in Ref. 3 thus removes roughly half of the discrepancy between theory and experiment, inasmuch as the experiment[9] indicates that the ^{48}Ca charge radius is 0.01 fm smaller than the ^{40}Ca charge radius. The fact that the form factor corrections to the ^{48}Ca charge radius found in this work are twice those found in Ref. 3 would be very encour-

TABLE II. Binding energies and rms radii of various distributions in ^{40}Ca, ^{48}Ca, and ^{208}Pb. Both proton (rms_p) and neutron (rms_n) rms radii are given for the point nucleon distributions as well as charge radii (rms_c) resulting from smearing the proton density with the Dirac form factor (*P-D*) and from smearing both proton and neutron densities with both Dirac and Pauli form factors (*PN-DP*).

	E/A		Point radii		rms_c		
Nucleus	Theo.	Exp.	rms_p	rms_n	*P-D*	*PN-DP*	Exp.
^{40}Ca	8.71	8.55	3.440	3.390	3.510	3.510	3.49
^{48}Ca	9.07	8.67	3.436	3.659	3.506	3.454	3.48
^{208}Pb	8.71	7.87	5.502	5.793	5.549	5.534	5.50–5.54

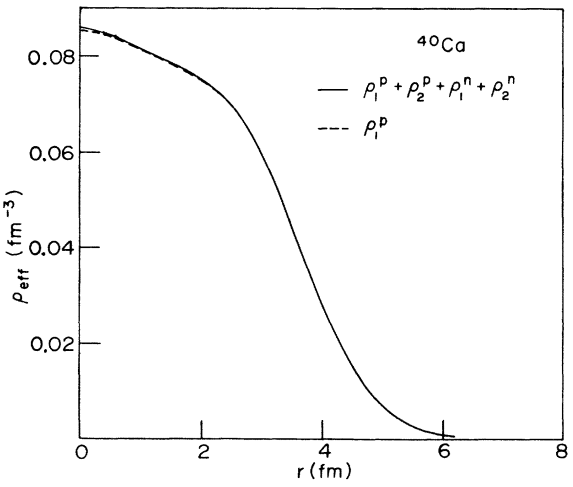

FIG. 3. The effective charge distribution of ^{40}Ca. The solid curve contains all form factor contributions, while the dashed curve contains only the contribution from the Dirac form factor of the protons.

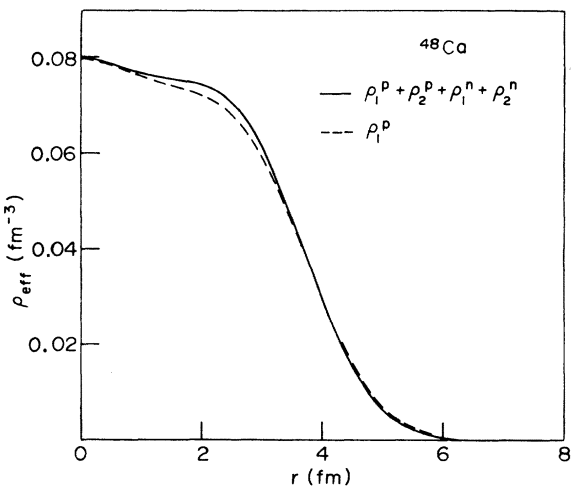

FIG. 4. The effective charge distribution of ^{48}Ca. The solid curve contains all form factor contributions, while the dashed curve contains only the contribution from the Dirac form factor of the protons.

aging were it not for the fact that, unlike Ref. 10, the present model gives a point proton radius in ^{48}Ca that is already 0.004 fm smaller than the ^{40}Ca point proton rms radius. In more recent calculations based on the methods of Negele and Vautherin,[11] the difference in point proton radii for ^{40}Ca and ^{48}Ca, using the model of Ref. 10, has decreased from 0.04 to 0.016 fm,[12] which is more like the result with the present model.

In Figs. 3 and 4 the effective charge distributions for ^{40}Ca and ^{48}Ca are shown. The solid curves contain the contributions from all nucleon form factors, while the dashed curves represent the contribution of the Dirac form factor of the proton only. As in the case of the rms radii, it is observed that the form factor corrections ($\rho_2^p + \rho_2^n + \rho_1^n$) almost vanish in the spin saturated ^{40}Ca nucleus, while they are quite noticeable for the spin unsaturated ^{48}Ca nucleus.

Figure 5 shows an example of the overall fit of the present model to the experimental differential cross section for the elastic scattering of 497 MeV electrons off ^{40}Ca. The experimental and theoretical curves differ by a small angular shift which increases as the scattering angle increases. This is the signature of the fact that the rms charge radius of the present model is about 0.025 fm larger than the preferred rms radius of the data. The positions and heights of the maxima are good, indicating that, aside from the overall need for a slightly smaller rms radius, the shape of the charge distribution of the present model is satisfactory. The theoretical model used in Fig. 5 has contributions from all form factors. The data are those of Heisenberg *et al.*[13]

In Fig. 6 the experimental isotopic shift[9] in the differential scattering cross sections of ^{40}Ca and ^{48}Ca is compared with the theoretical calculations both with (solid line) and without (dashed line) the

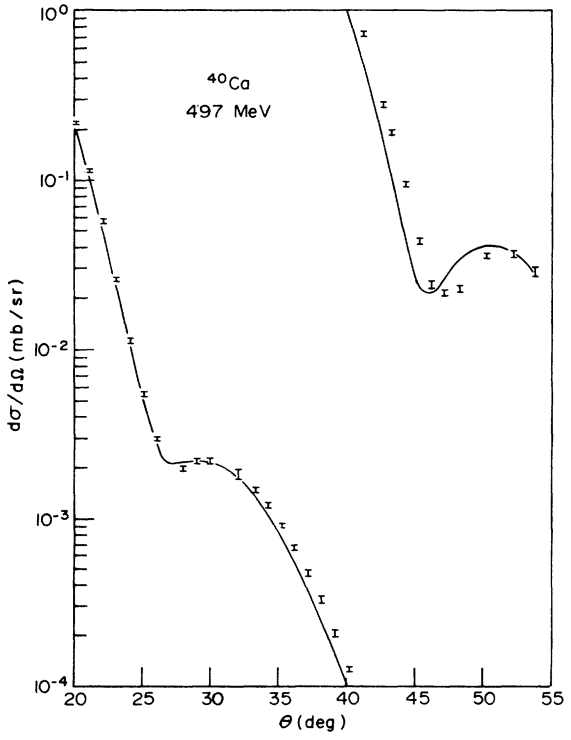

FIG. 5. Comparison between theory and experiment for the differential cross section for the elastic scattering of 497 MeV electrons off ^{40}Ca.

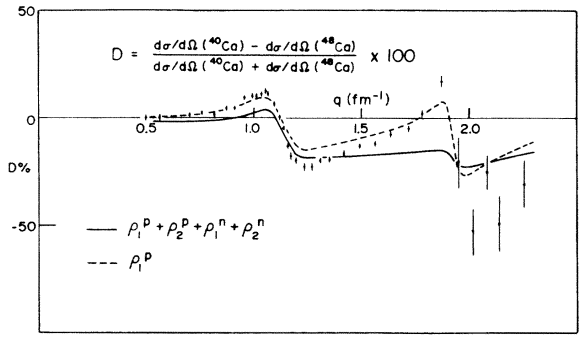

FIG. 6. Comparison between theory and experiment for the isotopic shift in the elastic differential scattering cross section of electrons off the ^{40}Ca and ^{48}Ca nuclei. The solid curve contains contributions from all form factors, while the dashed curve contains only the contribution of the Dirac form factor of the protons.

extra form factor corrections. As was indicated in the discussion of the rms matter radii, the present model actually gives better results when the form factor terms ρ_2^p, ρ_1^n, and ρ_2^n are not included.

The theoretical effective charge distribution of the ^{208}Pb nucleus is shown in Fig. 7. Again the solid line represents the contribution from all form factors, while the dashed line comes from the Dirac form factor contribution of the protons. The Dirac form factor contribution of the neutrons to the effective charge of ^{208}Pb is shown in Fig. 7 (multiplied by a factor of 10) by the dotted curve. Since multiplication of this term by a factor of 10 renders it comparable to the difference between the total charge densities with and without the form factor corrections, it is clearly a very small

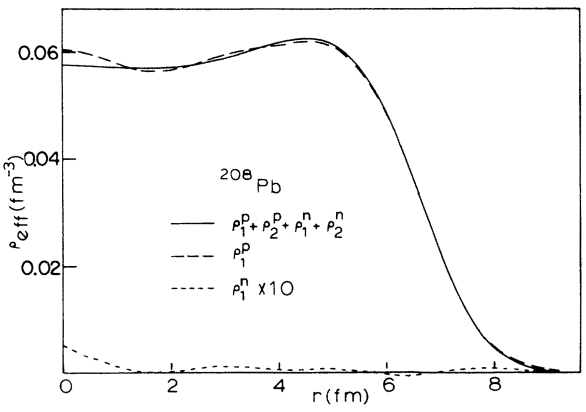

FIG. 7. The effective charge distribution of ^{208}Pb. The solid curve contains all form factor contributions, while the dashed curve contains only the contribution of the Dirac form factor of the protons. The dotted curve shows the contribution of the Dirac form factor of the neutrons multiplied by a factor of 10.

contribution to the overall charge density.

One interesting aspect of the curves shown in Fig. 7 is that the form factor corrections become larger as one approaches the origin and remove the central maximum (associated with the $3S\frac{1}{2}$ protons). This leaves a charge distribution with a distinct central depression, which was suggested in an earlier analysis of the experimental electron scattering cross sections of ^{208}Pb.[5] An earlier version of the present model has been considered previously by Friar and Negele.[14] They concluded that the central depression, which is noticeable even without the form factor corrections except for the s-state maximum, was due to an unrealistically small symmetry energy. This was not the case, as is shown by the present calculations

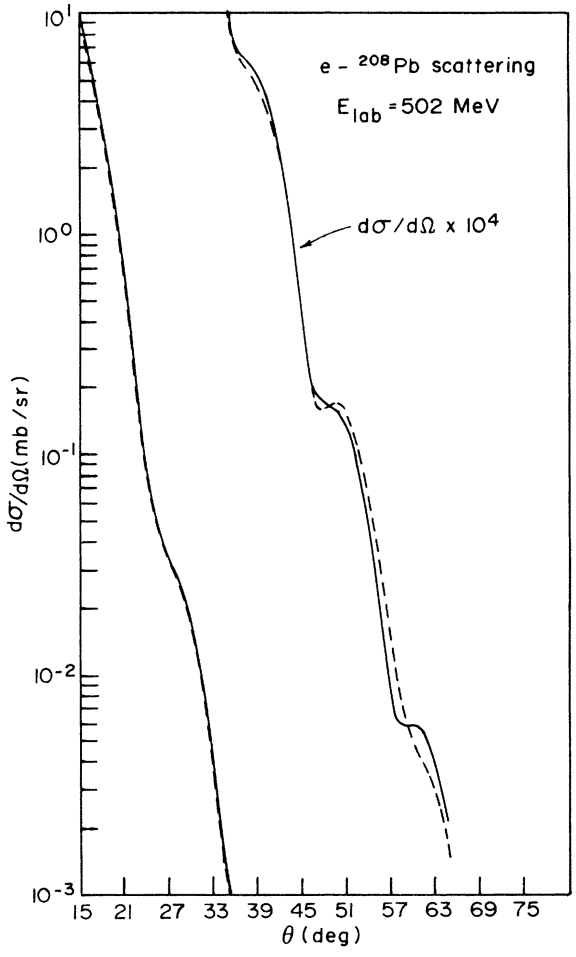

FIG. 8. Comparison between theoretical calculations of the elastic differential scattering cross section of 502 MeV electrons off ^{208}Pb. The solid curve uses a charge distribution which contains contributions from all form factors, while the dashed curve results from a charge distribution which contains only the contribution of the Dirac form factor of the protons.

which give the correct symmetry energy of infinite nuclear matter and yet still predict a charge density with a central depression. Nevertheless, the present model still overbinds the ^{208}Pb nucleus by 0.84 MeV/A, so the central depression may still vanish when the model is refined to give a more accurate description of the bulk properties of this nucleus.

As an example of the effects of the form factor corrections upon the elastic differential scattering cross sections, the cross sections for scattering of 502 MeV electrons from the ^{208}Pb charge distributions in Fig. 7 are shown in Fig. 8. The differences between the two curves become noticeable at the larger angles. The two charge distributions in Fig. 7 have been used to calculate electron scattering cross sections and muonic x-ray transitions for the broad range of experimental data considered by Friar and Negele[15] in their earliest study of the ^{208}Pb charge distribution. This data favors the curve in Fig. 7 which includes the form factor corrections over the curve without form factor corrections ($\rho_1^n+\rho_2^n+\rho_2^p$) by a factor of 2 in the total χ^2. The improvement in the χ^2 comes mainly from a better fit to the muonic x-ray data. Since muonic x-ray calculations are very sensitive to small changes in rms radii, it is not obvious whether the better fit is due to the shape change induced by the form factor corrections or simply due to the slight reduction in rms radius as shown in Table II. In order to answer this question the two charge densities in Fig. 7 have been scaled such that the rms radius of both is 5.505 fm, the radius preferred by the experimental data. Upon repeating the calculations with the scaled distributions, the situation is reversed with the ρ_1^p curve being favored over the full result by a factor of two in total χ^2. Within the present model calculations the data do not exhibit a clear preference for the form factor corrections. This same conclusion was reached recently by Chandra and Sauer.[16] They used a formalism similar to that of Ref. (3) and model ^{208}Pb wave functions of Kolb, Cusson, and Schmitt.[17]

V. CONCLUSIONS

A formalism is presented whereby the finite size effects of the nucleon electromagnetic form factors may be included in the calculation of effective nuclear charge distributions when the nuclear single-particle wave functions are Dirac spinors. In the special case where the nuclear distribution is radially symmetric, the contributions of the anomalous magnetic moment distributions are shown to be as simple and straightforward to include as the contributions of the charge form factors.

Numerical calculations are presented which display the relative importance of these form factor contributions for a particular local self-consistent nuclear model. The role which these form factor contributions play in understanding the isotopic shift anomaly in the ^{40}Ca-^{48}Ca charge distributions is discussed. The Pauli form factor contributions are shown to lead to a central depression in the ^{208}Pb charge distribution for the simple model employed. Comparisons of the model calculations with the various experimental data do not at this point show a clear preference for the inclusion of the Pauli form factor contributions in the effective charge distributions. Since the theoretical justifications for the inclusion of these effects are impeccable, one can only conclude that the nuclear model upon which these calculations are based must be refined before one can draw firm quantitative conclusions regarding the overall importance of these form factor contributions to the electromagnetic properties of nuclei.

ACKNOWLEDGMENT

The author is indebted to Dr. A. D. Jackson for clearing up certain questions concerning Ref. 4 and to Dr. A. Lande for providing the parameters of the form factor model used in this work, which were not published in Ref. 4. He is also indebted to Dr. J. Heisenberg for providing the experimental data on scattering of 497 MeV electrons off ^{40}Ca, which were used in Fig. 5, before their publication. He is further indebted to Dr. J. W. Negele for various discussions concerning the relationship between this work and that of Ref. 3, as well as for providing the computer codes which were used in the theoretical calculations of elastic electron scattering cross sections.

APPENDIX A

The purpose of this Appendix is to show that the last two terms of Eq. (21) vanish:

$$\left(\frac{\partial}{\partial\theta}+\cot\theta\right)\sum_i\left[\bar{\psi}_{N_i}\bar{\gamma}^0\bar{\gamma}^2\psi_{N_i}\right]+\frac{\partial}{\partial\phi}\sum_i\left[\bar{\psi}_{N_i}\bar{\gamma}^0\bar{\gamma}^3\psi_{N_i}\right]=0. \quad (1A)$$

In accordance with Ref. 2, the single nucleon wave functions are required to have the form

$$\psi(\vec{r})=\frac{1}{r}\begin{pmatrix}F(r) & \mathcal{Y}^{\omega}_{Jm}(\theta,\phi)\\ iG(r) & \mathcal{Y}^{-\omega}_{Jm}(\theta,\phi)\end{pmatrix}, \quad (2A)$$

where J and m are the usual angular momentum and magnetic quantum numbers, and ω is related to the parity of the state such that

$$P=(-1)^{J+\omega/2}. \tag{3A}$$

The $\mathcal{Y}^{\omega}_{Jm}(\theta,\phi)$ are central field spinors which are defined by

$$\mathcal{Y}^{\omega}_{Jm}(\theta,\phi)=\langle J+\tfrac{1}{2}\omega,\tfrac{1}{2},m-\tfrac{1}{2},\tfrac{1}{2}|Jm\rangle \times\mathcal{Y}_{J+\omega/2,m-1/2}(\theta,\phi)\begin{pmatrix}1\\0\end{pmatrix} +\langle J+\tfrac{1}{2}\omega,\tfrac{1}{2},m+\tfrac{1}{2},-\tfrac{1}{2}|Jm\rangle \times\mathcal{Y}_{J+\omega/2,m+1/2}(\theta,\phi)\begin{pmatrix}0\\1\end{pmatrix}. \tag{4A}$$

The $\mathcal{Y}_{lm}$ of Eq. (4A) are the usual spherical harmonics, and the notation for the two-component Pauli spinors is conventional. One should be reminded that the bar over the wave functions in Eq. (1A) represents the usual bar notation for Dirac spinors,

$$\bar{u}=(\gamma^0 u)^{\dagger}, \tag{5A}$$

while the bars over the Dirac matrices of Eq. (1A) indicate that the spherical coordinate γ matrices defined in Eq. (10) are being used.

Consider a term from the summation which is differentiated with respect to ϕ in Eq. (1A),

$$\frac{\partial}{\partial\phi}\{\bar{\psi}(\vec{r}),\bar{\gamma}^0\bar{\gamma}^3\psi(\vec{r})\}=\frac{\partial}{\partial\phi}\left\{\frac{1}{r^3\sin\theta}(F(r)\mathcal{Y}^{\dagger\omega}_{Jm}(\theta,\phi),iG(r)\mathcal{Y}^{\dagger-\omega}_{Jm}(\theta,\phi)\begin{pmatrix}0&\sigma_\phi\\\sigma_\phi&0\end{pmatrix}\begin{pmatrix}F(r)&\mathcal{Y}^{\omega}_{Jm}(\theta,\phi)\\iG(r)&\mathcal{Y}^{-\omega}_{Jm}(\theta,\phi)\end{pmatrix}\right\}. \tag{6A}$$

Upon performing the matrix products this becomes,

$$\frac{\partial}{\partial\phi}\{\bar{\psi}(\vec{r})\bar{\gamma}^0\bar{\gamma}^3\psi(\vec{r})\}=\frac{\partial}{\partial\phi}\{iF(r)G(r)[\mathcal{Y}^{\dagger\omega}_{Jm}(\theta,\phi)\sigma_\phi\mathcal{Y}^{-\omega}_{Jm}(\theta,\phi)+\mathcal{Y}^{\dagger-\omega}_{Jm}(\theta,\phi)\sigma_\phi\mathcal{Y}^{\omega}_{Jm}(\theta,\phi)]\}. \tag{7A}$$

Now using the relation,

$$\sigma_r\mathcal{Y}^{\omega}_{Jm}=-\mathcal{Y}^{-\omega}_{Jm}, \tag{8A}$$

and

$$\sigma_r\sigma_\phi\sigma_r=-\sigma_\phi, \tag{9A}$$

as well as the fact that σ_r is Hermitian, one can obtain

$$\frac{\partial}{\partial\phi}[\bar{\psi}(\vec{r})\bar{\gamma}^0\bar{\gamma}^3\psi(\vec{r})]=0. \tag{10A}$$

One obtains the same result for terms in the first summation of Eq. (1A) by reducing it to a form similar to Eq. (7A) and noting that Eq. (9A) holds when σ_θ is substituted for σ_ϕ. This establishes the validity of Eq. (1A).

APPENDIX B

The techniques of relativistic Hartree calculations for finite nuclei and infinite nuclear matter for the vector-scalar model considered here are thoroughly discussed in Refs. 1 and 2 and Ref. 7, respectively. A short review of these works is presented here.

For finite nuclei the single-particle wave functions ψ, which are used to calculate the effective charge distribution defined in Eq. (19), are obtained from numerical solutions to the following Dirac equation

$$\{\vec{\alpha}\cdot\vec{p}+\beta[M+U_s(\vec{r})+\gamma^0U_v^0(\vec{r})]\}\psi(\vec{r})=E\psi(\vec{r}). \tag{1B}$$

The single particle scalar (U_s) and vector (U_v^0) potentials are obtained by folding Yukawa functions associated with the meson parameters in Table I with the scalar and vector density distributions of the occupied positive energy states.

$$U_s(\vec{r})=-\sum_{\text{scalar mesons}}g_s^{\,2}\int\sum_i\bar{\psi}_i(\vec{r}')\psi_i(\vec{r}')\frac{e^{-\mu_s|\vec{r}-\vec{r}'|}}{|\vec{r}-\vec{r}'|}d^3r', \tag{2B}$$

$$U_v^0(\vec{r})=\sum_{\text{vector mesons}}g_v^{\,2}\int\sum_i\psi_i^{\dagger}(\vec{r}')\psi_i(\vec{r}')\frac{e^{-\mu_v|\vec{r}-\vec{r}'|}}{|\vec{r}-\vec{r}'|}d^3r'. \tag{3B}$$

This is an obvious relativistic analog of the nonrelativistic self-consistent Hartree approximation. For isoscalar mesons the contribution to the scalar potential is attractive while the contribution to the vector potential is repulsive.

For isovector mesons the expressions in Eqs. (2B) and (3B) must be altered to include an overall factor τ_3 (the third component of the isospin operator) and the density functions become the difference between the occupied neutron and proton states rather than the sum.

If the nucleus under consideration consists of closed shells, then the density functions are angle independent and the single-particle potentials U_s and U_v^0 become functions dependent only upon the radial coordinate r. For this case the single-particle wave function may be written in the form shown by Eq. (2A), where the large and small component radial wave functions F and G, respec-

tively, obey the radial form of the Dirac equation:

$$\frac{dF}{dr} = -\omega\frac{(J+\frac{1}{2})}{r}F + (M+U_s-U_v^0+E)G, \tag{4B}$$

$$\frac{dG}{dr} = (M+U_s+U_v^0-E)F + \omega\frac{(J+\frac{1}{2})}{r}G. \tag{5B}$$

The quantum numbers ω and J are those defined in Appendix A.

The analogous treatment of infinite nuclear matter has been given in Ref. 7. It is of interest in the present work because it allows the parameter search which resulted in the values shown in Table I to be constrained by the infinite nuclear matter parameters discussed in Sec. III.

For infinite nuclear matter the density functions and potentials in Eqs. (2B) and (3B) are constants

$$U_s = -\sum_{\text{scalar mesons}} g_s^2 \int \frac{e^{-\mu_s r}}{r} d^3r \left(\sum_i \bar{\psi}_i\psi_i\right), \tag{6B}$$

$$U_v^0 = \sum_{\text{vector mesons}} g_v^2 \int \frac{e^{-\mu_v r}}{r} d^3r \left(\sum_i \psi_i^\dagger\psi_i\right). \tag{7B}$$

For balanced nuclear matter characterized by a Fermi momentum k_F, the vector density is just the baryon density

$$\rho_B = \sum_i \psi_i^\dagger\psi_i$$
$$\rho_B = \frac{2}{3\pi^2}k_F^3. \tag{8B}$$

The scalar density is more complicated but can be written in the form

$$\rho_s = \frac{4}{(2\pi)^3}\int_0^{k_F}\frac{M+U_s}{[k^2+(M+U_s)^2]^{1/2}}d^3k, \tag{9B}$$

where use has been made of the properties of the solutions to the Dirac equation [Eq. (1B)] when U_s and U_v^0 are constants. If the integral in Eq. (9B) is performed and the result inserted into Eq. (6B), one obtains

$$U_s = -\left(\sum_{\text{scalar mesons}} g_s^2/\mu_s^2\right)\frac{4}{\pi}k_F^2(M+U_s) \times\left\{(1+a^2)^{1/2} - \tfrac{1}{2}a^2\ln\left[\frac{(1+a^2)^{1/2}+1}{(1+a^2)^{1/2}-1}\right]\right\}, \tag{10B}$$

where a is given by

$$a = \frac{M+U_s}{k_F}. \tag{11B}$$

Eq. (10B) may be solved numerically for the self-consistent scalar potential in terms of the Fermi momentum k_F and the model parameters (g_s^2/μ_s^2). The equation for the constant vector potential is

$$U_v^0 = \left(\sum_{\text{vector mesons}} g_v^2/\mu_v^2\right)\frac{8}{3\pi}k_F^3. \tag{12B}$$

The quantity of most interest in an infinite nuclear matter calculation is the saturation curve, or the binding energy per particle as a function of the Fermi momentum k_F. This can be obtained by conventional techniques for a sea of relativistic nucleons with momenta ranging from 0 to k_F and moving in the constant potentials U_s and U_v^0. The result is

$$E/A = U_v^0 - M + \tfrac{3}{8}k_F\left\{(1+a^2)^{3/2}+(1+a^2)^{1/2} - \tfrac{1}{2}a^4\ln\left[\frac{(1+a^2)^{1/2}+1}{(1+a^2)^{1/2}-1}\right]\right\} + \tfrac{3}{16}\pi\left(\sum_{\text{s.m.}}\frac{\mu_s^2}{g_s^2}\right)\frac{U_s^2}{k_F^3} - \tfrac{3}{16}\pi\left(\sum_{\text{v.m.}}\frac{\mu_v^2}{g_v^2}\right)\frac{(U_v^0)^2}{k_F^3}, \tag{13B}$$

where U_s and U_v^0 are the self-consistent potentials which satisfy Eqs. (10B) and (12B). Unlike the nonrelativistic theory of infinite nuclear matter which is unstable under scalar interactions in Hartree approximation, the result of Eq. (13B) is stable whether or not the repulsive vector exchanges are included.

One obtains from Eq. (13B) the result that the saturation curve for infinite nuclear matter depends upon only two combinations of the model parameters:

$$\alpha_s = \sum_{\text{s.m.}}\frac{\mu_s^2}{g_s^2}, \quad \alpha_v = \sum_{\text{v.m.}}\frac{\mu_v^2}{g_v^2}. \tag{14B}$$

where the sums are only over the isoscalar meson exchanges. Knowledge of the binding energy and the fermi momentum of the ground state of nuclear matter thus fixes the values of α_s and α_v and introduces two constraints on the parameter variations that are used for the finite nucleus calculations.

The infinite nuclear matter formalism provides a third constraint upon the model parameters which are associated with isovector meson exchanges. Such exchanges do not affect the calculation of balanced nuclear matter but do contribute when the fermi momenta associated with neutrons and protons become different. For the model shown in Table I, this constraint fixes completely the value of the coupling parameter of the ρ meson. The use of these three infinite nuclear matter constraints greatly simplified the parameter search which led to Table I.

*Work supported in part through funds provided by the U. S. Energy Research and Development Administration under Contract No. AT(11-1)3069.

† Present address: Department of Physics, University of Virginia, Charlottesville, Virginia 22901.

[1]L. D. Miller and A. E. S. Green, Phys. Rev. C 5, 241 (1972).

[2]L. D. Miller, Phys. Rev. C 1, 537 (1974).

[3]W. Bertozzi *et al.*, Phys. Lett. 41B, 408 (1972).

[4]F. Iachello, A. D. Jackson, and A. Lande, Phys. Lett. 43B, 191 (1973).

[5]J. Heisenberg *et al.*, Phys. Rev. Lett. 23, 1462 (1969).

[6]L. L. Foldy, Rev. Mod. Phys. 30, 471 (1958).

[7]J. D. Walecka, Ann. Phys. (N.Y.) 83, 491 (1974).

[8]J. H. E. Mattauch, W. Thiele, and A. H. Wapstra, Nucl. Phys. 67, 1 (1965).

[9]F. R. Frosch *et al.*, Phys. Rev. 174, 1380 (1968).

[10]J. W. Negele, Phys. Rev. C 1, 1260 (1970).

[11]J. W. Negele and D. Vautherin, Phys. Rev. C 5, 1472 (1972).

[12]J. W. Negele (private communication).

[13]J. Heisenberg (private communication).

[14]J. L. Friar and J. W. Negele, CTP Publication No. 456. The model considered in this work differed from the present model only in that the ρ meson coupling constant was 1.0 rather than 1.455.

[15]J. L. Friar and J. W. Negele, Nucl. Phys. A212, 93 (1973).

[16]H. Chandra and G. Sauer, Phys. Rev. C 13, 245 (1976).

[17]D. Kolb, R. Y. Cusson, and H. W. Schmitt, Phys. Rev. C 10, 1529 (1974).